

1 **PAH Concentrations Simulated with the AURAMS-PAH Chemical Transport**
2 **Model over Canada and the USA**

3
4
5 **E. Galarneau^{1,*}, P.A. Makar¹, Q. Zheng¹, J. Narayan¹, J. Zhang¹, M.D. Moran¹,**
6 **M.A. Bari^{1,2}, S. Pathela^{1,3}, A. Chen^{1,3}, and R. Chlumsky^{1,4}**

7
8 ¹ **Air Quality Research Division, Environment Canada, 4905 Dufferin Street,**
9 **Toronto, ON, M3H 5T4, Canada**

10
11 ² **Department of Public Health Sciences, School of Public Health, University of**
12 **Alberta, Edmonton, AB, T6G 2G7**

13
14 ³ **Department of Computer Science, University of Waterloo, 200 University Avenue,**
15 **Waterloo, ON, N2L 3G1, Canada**

16
17 ⁴ **Department of Environmental Engineering, University of Waterloo, 200 University**
18 **Avenue, Waterloo, ON, N2L 3G1, Canada**

19
20 *** Corresponding Author: Elisabeth Galarneau, elisabeth.galarneau@ec.gc.ca**

21
22
23
24
25
26
27 **Revised Manuscript**

28
29
30 **Submitted to**
31 **Atmospheric Chemistry and Physics**

32
33
34 **28 October 2013**

Abstract

35
36
37
38
39
40
41
42
43
44
45
46
47
48
49
50
51
52
53
54
55
56
57
58
59
60
61

The off-line Eulerian AURAMS (A Unified Regional Air quality Modelling System) chemical transport model was adapted to simulate airborne concentrations of seven PAHs: phenanthrene, anthracene, fluoranthene, pyrene, benz[a]anthracene, chrysene+triphenylene, and benzo[a]pyrene. The model was then run for the year 2002 with hourly output on a grid covering southern Canada and the continental USA with 42-km horizontal grid spacing. Model predictions were compared to ~5,000 24-hour-average PAH measurements from 45 sites, most of which were located in urban or industrial areas. Eight of the measurement sites also provided data on particle/gas partitioning which had been modelled using two alternative schemes. This is the first known regional modelling study for PAHs over a North American domain and the first modelling study at any scale to compare alternative particle/gas partitioning schemes against paired field measurements. The goal of the study was to provide output concentration maps of use to assessing human inhalation exposure to PAHs in ambient air. Annual average modelled total (gas + particle) concentrations were statistically indistinguishable from measured values for fluoranthene, pyrene and benz[a]anthracene whereas the model underestimated concentrations of phenanthrene, anthracene and chrysene+triphenylene. Significance for benzo[a]pyrene performance was close to the statistical threshold and depended on the particle/gas partitioning scheme employed. On a day-to-day basis, the model simulated total PAH concentrations to the correct order of magnitude the majority of the time. Model performance differed substantially between measurement locations and the limited available evidence suggests that the model spatial resolution was too coarse to capture the distribution of concentrations in densely populated areas. A more detailed analysis of the factors influencing modelled particle/gas partitioning is warranted based on the findings in this study.

62 1. Introduction

63
64 Polycyclic aromatic hydrocarbons (PAHs) are ubiquitous air pollutants that tend to be
65 most concentrated in areas of dense human population (Hafner et al., 2005) but are also
66 detected at locations remote from local sources (Hung et al., 2005). Many PAH species
67 have been classified as carcinogens (IARC, 2010) and they are implicated routinely as
68 toxicants in airborne particulate matter (Kelly and Fussell, 2012). They are regulated
69 under international agreements such as the Aarhus Protocol on Persistent Organic
70 Pollutants. Benzo[a]pyrene, a commonly-reported PAH species, is subject to ambient air
71 guidelines in many jurisdictions.

72
73 In Canada, PAHs meet the criteria for inclusion on the Toxic Substances List of the
74 Canadian Environmental Protection Act (Environment Canada and Health Canada,
75 1994), and the resulting government obligation has been to reduce or minimise their
76 release into the environment. Nationwide anthropogenic emissions of benzo[a]pyrene, a
77 commonly-reported species, fell by 70% between 1990 and 2010 according to estimates
78 made by the National Pollutant Release Inventory (Environment Canada, 2012). Though
79 there are no federal guidelines for PAHs in Canadian air, a recent analysis of ambient
80 monitoring data found that measured PAH concentrations regularly exceed the health-
81 based guidelines set by the Canadian province of Ontario (Galarneau and Dann, 2011).

82
83 In the USA, PAHs are listed as Clean Air Act Hazardous Air Pollutants as part of the
84 polycyclic organic matter (POM) class of compounds (US EPA, 2012) and have been
85 identified as a regional cancer concern in the US National-Scale Air Toxics Assessment
86 (US EPA, 2012). Industrial releases to air reported to the US Toxics Release Inventory
87 (TRI) fell by 35% between 1995 and 2010 (US EPA, 2012). There is no federal US
88 guideline for PAHs in ambient air.

89
90 PAH measurements are labour-intensive compared to those of criteria air contaminants
91 such as ozone and particulate matter, and the processes governing their atmospheric fate
92 are not yet well-understood. In an attempt to elucidate the spatiotemporal distributions of
93 PAH sources and ambient concentrations, several numerical modelling studies have been
94 published. Lagrangian frameworks have been used for Europe (Van Jaarsveld et al.,
95 1997; Halsall et al., 2001) and China (Liu et al., 2007; Lang et al., 2007; Lang et al.,
96 2008). Others studies have used box modelling (Prevedouros et al., 2004) and
97 multimedia fate approaches (Yaffe et al., 2001; Prevedouros et al., 2008). Eulerian
98 chemical transport models (CTMs) have been developed for Europe (Shatalov, 2005;
99 Aulinger et al., 2007; Matthias et al., 2009; Gusev et al., 2011; Bieser et al., 2012) and
100 east Asia (Zhang et al., 2009; 2011a; 2011b; Inomata et al., 2012), and three such studies
101 on a global scale have also been published in recent years (Sehili and Lammel, 2007;
102 Lammel et al., 2009; Friedman and Selin, 2012).

103
104 The aforementioned studies differ in many respects relating to the PAH species
105 examined, the temporal variability of their emissions, and the spatial resolutions and
106 process representations in the models. None has focussed exclusively on North America
107 at the regional scale. As well, although several particle/gas partitioning mechanisms have
108 been explored in other models, including Junge-Pankow adsorption (Junge, 1977;

109 Pankow, 1987), organic matter sorption (Finizio et al., 1997), and combined
110 adsorption/absorption (Dachs and Eisenreich, 2000), no previous studies have evaluated
111 model output against paired phase-distributed measurements for alternative partitioning
112 expressions on the same domain.

113
114 This study presents the results of a chemical transport model, AURAMS-PAH, run over
115 North America at 42-km horizontal grid spacing with hourly output for the year 2002.
116 Seven PAH species were simulated with the model. Three isomer pairs of decreasing
117 volatility and increasing particulate fraction comprise six of the species: phenanthrene
118 (PHEN) and anthracene (ANTH) (178 g mol^{-1}), fluoranthene (FLRT) and pyrene (PYR)
119 (202 g mol^{-1}), and benz[a]anthracene (BaA) and chrysene/triphenylene (C+T) (228 g mol^{-1}).
120 The seventh PAH, benzo[a]pyrene (BaP) (252 g mol^{-1}), is not generally considered to
121 be semivolatile but has been included due to its common use as a representative PAH
122 species. Two particle/gas partitioning schemes, Junge-Pankow (JP: Junge, 1977;
123 Pankow, 1987) and Dachs-Eisenreich (DE: Dachs and Eisenreich, 2000), were tested.

124
125 Model performance was evaluated against ~5,000 measurements from 45 stations in
126 established networks in Canada and the USA. This is the first published model to be run
127 and evaluated for PAH concentrations and their distributions between the particle and gas
128 phases using two partitioning methods. It is also the first such model to be evaluated
129 over a regional North American domain.

130

131 **2. Methods**

132

133 **2.1 Model Description**

134

135 AURAMS (A Unified Regional Air quality Modelling System) is an Eulerian CTM
136 originally developed to simulate criteria air contaminants. The standard version of the
137 model uses a sectional approach to represent the size distribution of airborne particles: 12
138 size bins from 0.01 to 40.96 μm in diameter and 9 particulate species (sulphate, nitrate,
139 ammonium, elemental carbon, primary organic aerosol, secondary organic aerosol,
140 crustal material, sea salt, and aerosol water) are usually considered. The model includes
141 process representation for tropospheric gas-phase oxidative chemistry, the absorptive
142 formation of secondary organic aerosols, inorganic heterogeneous chemistry, particle
143 microphysics (nucleation, condensation, coagulation, etc.), cloud processing of aerosols,
144 advective transport, vertical diffusion, and gas and particle emissions and deposition. A
145 detailed overall description of AURAMS appears in Gong et al. (2006) while a
146 description of the aerosol sectional approach and the microphysics modules of the model
147 can be found in Gong et al. (2003a,b). Performance evaluation and model
148 intercomparison results for AURAMS appear in McKeen et al. (2008), Smyth et al.
149 (2009), Makar et al. (2010), Kelly et al. (2012) and Solazzo et al. (2012) among other
150 publications.

151

152 A modified version of the AURAMS CTM known as AURAMS-PAH was developed to
153 incorporate primary semivolatile organic compounds that are subject to sorptive
154 partitioning. Starting from the standard AURAMS CTM had the advantage that a

155 number of required fields for modelling PAHs were already available. These included
156 hydroxyl concentration, total particle surface area, and fractions of particle elemental
157 carbon and organic carbon. The modifications made to AURAMS version 1.3.2 in order
158 to simulate PAHs are described below. Physico-chemical property values used for each
159 PAH in the modified code are found in Table S1.1 of the Supplementary Material.

160

161 *2.1.1 Dry Deposition of Gases.* Within AURAMS, gaseous dry deposition velocities are
162 modelled using the inverse resistance analogy for several land-use categories (Zhang et
163 al., 2002). Three resistances are assessed in AURAMS and only the first of these
164 (aerodynamic resistance) is independent of the chemical species under consideration.
165 The species-dependent resistances are the quasi-laminar sub-layer resistance and the
166 surface or canopy resistance. The latter both depend on the gas-phase diffusivity of the
167 compound in question, and this quantity was calculated in the model according to the
168 Fuller et al. method described in Reid et al. (1987).

169

170 Surface or canopy resistance is the most complex of the three gaseous dry deposition
171 component resistances and tends to dominate total dry deposition (Zhang et al., 2002).
172 One of its sub-components, mesophyll resistance, was set to 100 s m^{-1} for species that are
173 relatively insoluble in water and have small oxidizing capacities, as is the case for PAHs.
174 The remaining sub-components (cuticle and ground resistances) are determined by
175 scaling to O_3 and SO_2 settings based on physico-chemical qualifications. For the PAHs,
176 scaling factors to O_3 and SO_2 for both acetaldehyde and C_3 carbonyls, the least soluble
177 organic compounds considered in AURAMS aside from the PAHs, were used.
178 Unsubstituted compounds such as PAHs are generally considered to have high
179 resistances to deposition whereas carbonyl resistances are thought to be lower (Zhang et
180 al., 2002). However, published observations of PAH deposition led us to assume that
181 deposition velocities would be greater than zero (low resistances) and we therefore used
182 the best-available homologues in AURAMS to represent PAHs. This is an uncertainty in
183 the model that merits future attention.

184

185 Volatilisation of gaseous PAHs can occur from exposed water (Hoff et al., 1996), soil
186 (Jones, 1994), and impervious urban surfaces (Diamond et al., 2000). Net gaseous
187 deposition to the Great Lakes in 2002 was downward (Blanchard et al., 2005) suggesting
188 that PAH fugacities in air exceeded those in surface compartments at the regional scale.
189 Volatilisation was not included in this first-generation version of AURAMS-PAH and the
190 effect of this omission is presented in Section 3.1.1.

191

192 *2.1.2 Gas-Phase Reactions.* Reactions of gas-phase PAHs with hydroxyl radicals are
193 considered in this model. Since these reactions consume relatively little hydroxyl due to
194 the trace concentrations of PAH, their reactions were simulated outside the AURAMS
195 gas-phase chemistry solver. PAH oxidative loss was estimated as a first-order process
196 using the model-predicted OH concentration immediately preceding particle-gas
197 partitioning. Only seven new gas-phase concentration fields were added to the CTM;
198 PAH reaction products were not tracked in the model, either as individual gas-phase
199 species or as contributors to SOA.

200

201 Hydroxyl reaction rate constants were taken from the program AOPWIN which is part of
202 the US EPA's EPI Suite (U.S. EPA, 2006). Measured constants are available for three
203 low-molecular-weight PAHs considered here (phenanthrene, anthracene, fluoranthene)
204 and these values were represented in AOPWIN. However, measurements for the
205 remaining four PAHs are not available and the software predicted the same hydroxyl
206 reaction rate constant of $50 \times 10^{-12} \text{ cm}^3 \text{ molec}^{-1} \text{ s}^{-1}$ for these species.

207

208 *2.1.3 Particle Representation of PAHs.* Seven additional particle species, each with 12
209 size bins as in the original AURAMS configuration, were added to the model to represent
210 the particle-bound PAH mass.

211

212 *2.1.4 Particle/Gas Partitioning of PAHs.* A new algorithm was developed for
213 AURAMS-PAH to account for the sorptive particle/gas partitioning of PAHs. It is fully
214 adaptable to other semivolatile species with similar atmospheric partitioning behaviour to
215 PAHs such as dioxins and furans, PCBs, and organochlorine pesticides. The partitioning
216 of PAHs to airborne particles was assumed to be fully reversible.

217

218 Two instantaneous equilibrium sorptive partitioning expressions were incorporated in the
219 new partitioning subroutine. The first treated particle/gas partitioning as a Langmuirian
220 adsorption process on a uniform particle surface (JP: Junge, 1977; Pankow, 1987). The
221 model calculations began by adding the particulate PAH concentrations in all size bins
222 (ΣC_p) and the gas-phase PAH concentration (C_g) to give a total PAH concentration
223 (C_{TOT}) for each species. An updated bulk particulate fraction (ϕ) was then assigned
224 according to the first part of Eq. (1):

225

$$\phi = \frac{c \Sigma \theta}{c \Sigma \theta + p_L^0} = \frac{\Sigma C_p}{C_{TOT}}, \quad (1)$$

226

227 where c is a constant set at 0.173 J m^{-2} (estimated from Figure 3 in Junge, 1977), $\Sigma \theta$ is
228 the total particle surface area concentration ($\text{m}^2 \text{ m}^{-3}$) and p_L^0 is the saturated vapour
229 pressure of the sub-cooled liquid (Pa) taken from the temperature-dependent values
230 measured by Offenberg and Baker (1999; see Table S1.1). We have selected Junge's
231 (1977) value of c over that estimated by Pankow (1987) since the latter was based on
232 assumptions that have not been revisited in light of the numerous observations of PAH
233 partitioning published since. The total particulate PAH concentrations dictated by ϕ were
234 then redistributed among the particle size bins by prorating to the proportion of total
235 aerosol surface area concentration within each size bin. The redistributed gas-phase PAH
236 concentration was determined by difference between C_{TOT} and ΣC_p .

237

238 The second equilibrium partitioning expression available in the partitioning subroutine
239 developed a partition coefficient ($K_p, \text{m}^3 \mu\text{g}^{-1}$) based on the contributions of two additive
240 processes: absorption into particulate organic matter and adsorption onto particulate soot
241 (DE: Dachs and Eisenreich, 2000)

242

$$K_p = 10^{-12} (1.5 f_{OC} / \rho_{oct} K_{OA} + f_{EC} K_{SA}) = \frac{(\sum C_p / C_{TSP})}{C_g}, \quad (2)$$

243

244 where ρ_{oct} is the bulk density of octanol (0.82 kg L^{-1}), f_{OC} is the organic carbon fraction
 245 of the particulate matter (the 1.5 multiplier converts organic carbon to organic matter
 246 which is assumed to be well-represented by octanol), K_{OA} is the octanol-air partition
 247 coefficient (dimensionless), f_{EC} is the elemental carbon fraction of the particulate matter,
 248 K_{SA} is the soot-air partition coefficient (L kg^{-1}), $\sum C_p$ is the particulate PAH concentration
 249 across all the size bins (ng m^{-3}), C_{TSP} is the total particulate matter concentration ($\mu\text{g m}^{-3}$),
 250 and C_g is the gas-phase concentration (ng m^{-3}).

251

252 Soot-air partition coefficients (K_{SA} , L kg^{-1}) were estimated as the ratios of soot-water
 253 (K_{SW}) to air-water partition (K_{AW}) coefficients since direct K_{SA} measurements are not
 254 available for PAHs. K_{SW} values from Jonker and Koelmans (2002) were used in this
 255 model. These values vary substantially (up to a factor of 47) between relevant soots for
 256 each PAH considered here. Since a single K_{SW} was needed for each PAH in the model,
 257 representative values were determined by weighting the reported K_{SW} values by the
 258 contribution of their related combustion processes to the total emitted fine particulate
 259 matter ($\text{PM}_{2.5}$) used in the inventory of Galarneau et al. (2007). Temperature-dependent
 260 K_{AW} values were taken from Bamford et al. (1999). K_{OA} values were taken from the
 261 temperature-dependent expressions determined by Odabasi et al. (2006).

262

263 PAH partition coefficients were calculated according to the first part of Eq. (2). By
 264 determining the contribution of each size bin's organic matter and soot carbon to the
 265 totals across all size bins, the total particulate PAH was apportioned to each size bin. For
 266 example, if a total partition coefficient had contributions from the organic matter and soot
 267 carbon of 20% and 80%, respectively, and size bin 1 held 10% of the total particulate
 268 organic matter and 15% of the total soot carbon, the fraction of total particulate PAH
 269 assigned to size bin 1 would be 14% (viz., $0.2 \times 0.1 + 0.8 \times 0.15$). Gas-phase
 270 concentrations were then determined by difference between C_{TOT} and $\sum C_p$.

271

272 *2.1.5 Below-cloud (Precipitation) Scavenging.* Scavenging of gas and particle PAHs by
 273 liquid precipitation was calculated as per Gong et al. (2006). Particle scavenging
 274 assumed that particle-bound PAHs do not dissolve in falling rain; particle-bound PAHs
 275 were thus treated as passive aerosol tracers. Snow scavenging of gaseous PAHs was not
 276 considered in this version of AURAMS though particle-bound PAHs are scavenged by
 277 snow in the model as passive components of airborne particles.

278

279 *2.1.6 Cloud Processing.* Cloud processing in the model was treated in a similar manner
 280 to precipitation scavenging whereby gas-phase mass transfer to cloud water is species-
 281 dependent, whereas particulate interactions with cloud droplets are only affected by the
 282 presence of PAHs in terms of the size (mass and volume) that they represent as part of
 283 the overall aerosol. Solid-phase densities used to relate aerosol PAH mass to volume
 284 were taken from Mackay et al. (2006; see Table S1.1).

285

286 **2.2 Model Domain, Emissions, and Boundary Conditions**

287

288 The model domain included southern Canada and the continental USA (see Figure 1). It
289 was run on a 42-km polar stereographic grid using off-line meteorology generated with
290 the Global Environmental Multiscale numerical weather prediction model (GEM v 3.2.0:
291 Côté et al., 1998a, b).

292

293 Emissions of PAHs were taken from the inventory of Galarneau et al. (2007) that had
294 been updated from 2000 to 2002 and to which benzo[a]pyrene had been added using
295 identical methods and data sources. As discussed in Galarneau et al. (2007), hourly PAH
296 emissions fields were estimated with an emissions processing system using source-
297 specific temporal profiles. The temporal profile library included 3020 month-of-year, 64
298 day-of-week, and 2672 hour-of-day temporal profiles for Canada and 1500, 49, and 680
299 analogous temporal profiles for the US. The overall temporal profile thus varies from
300 grid cell to grid cell due to the different mixtures of source types found in each one.

301

302 All PAHs were emitted exclusively in the gas phase. Particle/gas partitioning took place
303 at each 15-minute CTM time step according to the partitioning module described in
304 Section 2.1.5. As mentioned in Section 2.1.2, no emissions of previously deposited
305 PAHs were considered in this first-generation version of the model and the implications
306 of this are discussed in Section 3.1.1. Emissions of SO₂, NO_x, NH₃, CO, volatile organic
307 compounds (VOCs), and particulate matter were derived using Environment Canada and
308 US EPA databases and methods for the year 2002.

309

310 Initial PAH concentrations at all lateral boundaries were set to zero in anticipation of
311 pronounced spatial gradients away from localised source regions. As a result, modelled
312 concentrations in Mexico and near its border with the US are not expected to be reliable,
313 particularly since PAH emissions from Mexico have not been included in the model.
314 Model output along the northern edge of the domain over western Canada is similarly
315 expected to be unreliable since emission sources are located close to the model boundary
316 in that region. The development of representative non-zero boundary concentrations is
317 anticipated as part of future model development.

318

319 **2.3 Evaluation Data**

320

321 Observational PAH data used for comparison with model output were collected from four
322 measurement networks: NAPS (Canada), IADN (Canada-US), CARB (California), and
323 Rio Tinto Alcan (Kitimat, British Columbia, Canada). The measurement stations are
324 depicted in Figure 2 and described in Section 2 of the Supplementary Material.

325

326 Measurement data were available from a total of 45 stations, 23 in Canada and 22 in the
327 USA, all of which collected samples integrated over periods of 24 hours. Particle/gas
328 partitioning was assessed at eight stations, three in Canada and five in the USA, all of
329 which were operated by IADN.

330

331 The IADN phase-distributed data were also combined to yield total concentrations.
332 These combined IADN data, along with NAPS and Rio Tinto data, yielded a total of 28
333 sites at which total PAH concentration for all the modelled PAHs could be assessed.

334 Particulate PAH measurements from the latter networks were determined from samples
 335 of total suspended particles (TSP). CARB provided data for benzo[a]pyrene in particles
 336 smaller than 2.5 µm in diameter (PM_{2.5}) at a further 17 locations.

337
 338 Four model grid squares (Kitimat, Toronto, Hamilton, and Montreal) contained two or
 339 more measurement stations thus allowing for an assessment of the adequacy of modelling
 340 all seven PAHs at 42-km grid spacing.

341

342 **3. Results**

343

344 **3.1 Total PAH Concentration**

345

346 **3.1.1 Overall Spatiotemporal Domain**

347

348 Total PAH concentration refers to the sum of the gas and particulate concentrations
 349 whether these have been analysed together (e.g., NAPS) or separately (e.g., IADN). For
 350 stations at which the gas and particle phases were analysed separately, a valid total
 351 concentration was assumed to exist if at least one of the gas and particle phase
 352 concentrations was greater than the detection limit. Non-detectable values were assumed
 353 equal to zero for the calculation of total concentrations.

354

355 A representative plot of the spatial distribution of modelled annual average
 356 concentrations is presented in Figure 1 for fluoranthene. The remaining PAHs show
 357 similar spatial distributions and maps of their modelled concentrations are found in
 358 Section 3 of the Supplementary Material. All the PAHs show spatial distributions of
 359 their modelled concentrations that are consistent with regional dispersion of their
 360 emissions as depicted in Galarneau et al. (2007).

361

362 A summary of annual mean modelled and measured values over the entire spatiotemporal
 363 model domain is shown in Table 1. Only modelled values for which there was a
 364 corresponding measurement were included.

365

366 **Table 1:** Summary of 2002 Annual Modelled and Measured Total PAH Concentration
 367 Mean (Standard Deviation) Values (ng m⁻³)

368

PAH	Modelled – JP	Modelled - DE	Measured	n ¹
PHEN	12.75 (36.44)	12.76 (36.44)	36.06 (131.8)	790
ANTH	0.9123 (1.757)	0.9104 (1.759)	2.804 (11.56)	701
FLRT	6.781 (14.40)	6.888 (14.66)	9.179 (32.44)	789
PYR	5.727 (12.23)	6.009 (13.40)	5.733 (21.57)	785
BaA	1.227 (2.438)	1.328 (2.704)	1.326 (6.081)	610
C+T	1.511 (3.964)	1.473 (3.569)	3.303 (21.95)	721
BaP	1.173 (2.002)	1.424 (2.455)	0.9047 (3.238)	595

369 ¹n = number of modelled-measured data pairs

370

371 In comparing modelled results to measurements, the annual means were statistically
 372 indistinguishable at the 95% confidence level for FLRT, PYR, BaA, and BaP (JP)
 373 whereas they were statistically different for PHEN, ANTH, C+T, and BaP (DE). For

374 PHEN, ANTH, and C+T, modelled values were underestimated relative to measurements
375 whereas they were overestimated for DE BaP.

376

377 The model's temporal variability tended to be smaller than that of the corresponding
378 measurements; the relative standard deviations of the measurements were 1.3 to 2.7 times
379 greater than those of the modelled values. A similar observation has been made in the
380 modelling of particulate matter with AURAMS and other regional air quality models
381 (Solazzo et al., 2012) For PAHs, this effect was also seen by Matthias et al. (2009) who
382 concluded that temporal variability in PAH emissions was not adequately represented by
383 their inventory. This is a plausible contributing factor in the current study as well.
384 Furthermore, meteorological parameters vary over a scale much finer than that used for
385 regional air quality models. As a result, observed concentrations from point locations can
386 be expected to exhibit greater variability than modelled concentrations determined for
387 entire grid squares.

388

389 Differences in mean modelled total concentrations between the two partitioning versions
390 (JP and DE) were statistically indistinguishable at 95% significance despite the finding
391 that the two BaP model results differed in their comparison to measured values. The
392 latter anomaly indicates that the BaP distributions were close to the 95% confidence
393 threshold. As a result, no conclusion can be drawn about which partitioning mechanism
394 was superior in simulating overall total PAH concentrations. Phase partitioning of
395 semivolatile organic compounds (SVOCs) is a major determinant of their potential for
396 long-range transport (Bidleman, 1988), yet it does not appear to have a large effect on the
397 simulation of their total concentrations at the regional scale. Model performance in
398 simulating phase partitioning is discussed in Section 3.2.

399

400 The model's performance was also more closely evaluated by examining the pertinent
401 data distributions. Figure 3 depicts frequency distributions of the ratios of modelled-to-
402 measured concentrations for all of the valid data pairs available for the model evaluation.
403 Four PAH species (ANTH, FLRT, PYR, and C+T) yielded median values of the
404 modelled-to-measured concentration ratio that were close to the ideal value of unity (1.1,
405 1.1, 1.5, and 1.4, respectively). PHEN showed an overall tendency toward
406 underestimation by the model (0.2), whereas BaA and BaP tended toward overestimation
407 (3.2/3.5 and 3.0/3.5 JP/DE, respectively).

408

409 BaA and BaP are reactive PAHs (e.g., Behymer and Hites, 1985; Pöschl et al., 2001;
410 Kwamena et al., 2004; Esteve et al., 2006, Shiraiwa et al., 2009) and the exclusion of
411 particle-bound reactions in this first-generation model may explain a portion of their
412 overestimation in AURAMS-PAH as suggested in a comparable model for Europe
413 (Matthias et al., 2009). However, BaP is subject to losses during sampling (Menichini,
414 2009) and some portion of the apparent model overestimation may in fact be due to
415 measured concentrations that are biased low since the samplers used were not equipped
416 with oxidant denuders. This presents a priority for future research since many
417 jurisdictions use BaP as an indicator PAH when setting air quality standards.

418

419 As presented in Section 2.1.2, volatilisation of gaseous PAHs from surface compartments
420 such as water and soil was not included in this first-generation version of AURAMS-

421 PAH. If such volatilisation were significant to the balance of PAHs in ambient air
422 relative to the other processes simulated, one would expect an overall bias in model
423 results whereby the most volatile PAHs, which are found predominantly in the gas phase,
424 would be underestimated and the least volatile particulate species would be unaffected.
425 Summary results provide indefinite evidence. Volatile phenanthrene is systematically
426 underestimated yet its similarly volatile isomer, anthracene, shows an ambiguous central
427 tendency whereby its mean concentrations are underestimated by the model (Table 1) but
428 its median concentrations are not (Figure 3). Less volatile but nonetheless predominantly
429 gaseous fluoranthene and pyrene show no tendency toward underestimation. These
430 results warrant further investigation but suggest that volatilisation of gaseous PAHs from
431 surface compartments may not be significant at the regional scale when model results are
432 compared to 24-hour measurements from predominantly urban locations. This finding
433 stands in contrast to the reported importance of air-surface exchange at remote locations
434 determined through global-scale modelling (Lammel et al., 2009).

435
436 The range of modelled-to-measured concentration ratios shown in Figure 3 varied
437 substantially by species. The ratios of 90th to 10th percentile values for PHEN, FLRT,
438 PYR, BaA, and C+T spanned fewer than, or close to, two orders of magnitude (55, 59,
439 67/68, 67/63, and 100/93, respectively). The ratio for BaP was larger (180/270) and that
440 for ANTH was very large (5900/7400), with extreme values tending toward
441 underestimation for the latter species. As seen with the comparison of means, the two
442 partitioning parametrizations used by AURAMS-PAH led to similar model performance
443 overall when considering the distribution of total PAH concentrations.

444
445 Additional quantitative performance metrics are presented for the two particle/gas
446 partitioning parametrizations in Tables S4.1 and S4.2 of the Supplementary Material.
447 Normalized mean bias and error have been included for completeness, but their utility in
448 this evaluation is questionable given the large range of concentrations. Measured
449 maximum to minimum concentration ratios range from 4.7E+06 (PYR) to
450 1.3E+09/1.4E+09 (C+T). Therefore, the mean measured concentrations used to
451 normalize the bias and error do not represent the dataset well.

452
453 The correspondence between individual modelled-measured data pairs is weak as
454 demonstrated by the low coefficients of determination, non-unity slopes, and high
455 intercepts listed in Tables S4.1 and S4.2. However, the ability of the model to simulate
456 observed concentrations within a certain tolerance is reasonable, especially when
457 considering that PAHs are trace organic compounds subject to numerous sampling
458 artefacts (McDow, 1999) and poor measurement precision (Galarneau, 2008).
459 Depending on PAH species, 22-34% of modelled-measured data pairs fell within a factor
460 of 2 of each other. This increased to 61-86% when considering a factor of 10. As a
461 result, it can be stated with confidence that, on average, AURAMS-PAH was able to
462 simulate atmospheric PAH concentrations in North America for rural to urban locations
463 to the correct order of magnitude.

464 465 **3.1.2 Site-Specific Performance**

466

467 Model performance was not spatially uniform. Figure 4 depicts the variation in
468 distributions of individual modelled-to-measured concentration ratios across
469 measurement sites for fluoranthene, the PAH species for which overall performance was
470 best as determined by the median and spread in modelled-to-measured concentration
471 ratios. Note that only JP partitioning values have been plotted since these are visually
472 indistinguishable from those for DE partitioning.

473
474 Of the 30 sites depicted in Figure 4 (CARB sites could not be considered since only
475 benzo[a]pyrene was reported there), the median modelled-to-measured concentration
476 ratio ranged from 0.061 (St. John's) to 4.0 (Hamilton – Confederation Park), whereas the
477 median value for all sites was 1.1. The variability at individual sites is itself highly
478 variable, with ratios of 90th to 10th percentile values of the modelled-to-measured
479 concentration ratio ranging from 5.8 (Toronto – Junction Triangle) to 105,000 (Haul
480 Road, near the Rio Tinto Alcan smelter in Kitimat, British Columbia). A low value of
481 1.1 was observed for Saint John, but this was based on only two modelled-measured data
482 pairs. Sixteen of the 30 sites (53%) had median modelled-to-measured ratios that fell
483 within a factor of two of the median value for all sites.

484
485 The other compounds varied spatially in a manner similar to fluoranthene with the
486 following exceptions. ANTH exhibited atypically large underestimation at the three sites
487 near the Rio Tinto Alcan smelter in Kitimat, suggesting that inaccurately low ANTH
488 emissions are associated with the dominant source there. The reporting threshold for
489 point-source ANTH emissions through the Canadian National Pollutant Release
490 Inventory (NPRI) system is higher than the thresholds for other commonly-measured
491 PAHs and no ANTH emissions were reported to the NPRI by Rio Tinto Alcan for 2002.
492 The C+T performance at Jonquière, home to aluminum smelting facilities, suggests that
493 reported emissions there are also too low. Emissions for other PAHs were reported from
494 this location for 2002 but not so for chrysene, which is called benzo[a]phenanthrene in
495 the NPRI.

496 **3.1.3 Model Grid Squares Containing Multiple Measurement Sites**

497
498
499 The smoother the spatial distribution of a pollutant, the coarser the model resolution that
500 can be used to simulate it. Four AURAMS-PAH model grid squares contain more than
501 one measurement site, thus allowing for an assessment of the 42-km spatial resolution
502 used for the evaluation runs. The multi-site grid squares are all located in Canada, and
503 from west to east, they encompass sites in Kitimat (2 sites), Hamilton (2), Toronto (3),
504 and Montreal (2) (see Tables S2.1 and S2.4).

505
506 Kitimat is a town 650 km northwest of Vancouver with approximately 9,000 residents
507 whose largest employer is the aluminum smelter complex operated by Rio Tinto Alcan
508 (District of Kitimat, 2009). Two measurement sites (Haul Road and Kitimaat Village)
509 are located in the same model grid square and a third site (Whitesail) lies in an adjacent
510 square even though it is only a few kilometers away. Hamilton is a city at the western
511 end of Lake Ontario that is known colloquially as the Steel Capital of Canada and had a
512 population of approximately 700,000 in 2010. It is part of the so-called “Golden
513 Horseshoe” conurbation at the western end of Lake Ontario whose 2010 population,

514 estimated as the sum of the populations of Oshawa, Toronto, Hamilton, and St.
 515 Catharines-Niagara, was over 7 million (Statistics Canada, 2011). Toronto and Montreal
 516 are the largest cities in Canada having 2010 populations of 5.7 and 3.9 million,
 517 respectively.

518
 519 Table 2 lists the variability in contemporaneously measured concentrations at the four
 520 grid squares as represented by their coefficients of variation (COV). At any given site,
 521 the average COVs for the different PAH species tend to be similar to each other.
 522 Substantial differences exist between sites, however, particularly when grouping the
 523 urban sites (Hamilton, Toronto, and Montréal) against the industrial site at Kitimat. This
 524 is not unexpected. Urban areas include complex mixtures of point, area, and mobile
 525 sources that are distributed over distances similar to the scale of the model. Kitimat
 526 houses industrial operations within a relatively small area of otherwise rural land and
 527 wilderness. Steep spatial gradients in pollutant concentrations are expected there as a
 528 result.

529
 530 **Table 2: Average Coefficient of Variation (%) between Contemporaneous**
 531 **Measurements at Sites Falling Within the Same 42-km AURAMS-PAH Grid Square**
 532

Station	PHEN	ANTH	FLRT	PYR	BaA	C+T	BaP	O ₃ ²	TSP
Kitimat	106	101	96.5	93.7	87.4	91.3	93.2	N/A	N/A
Hamilton	52.1	59.0	59.2	58.8	73.1	117	62.8	24.9	30.5
Toronto3 ¹	36.2	48.7	42.5	39.6	42.2	32.9	43.0	N/A	22.1
Toronto2 ¹	36.5	45.4	39.3	35.7	32.9	25.0	38.0	12.2	24.6
Montréal	49.2	52.9	45.8	44.6	55.2	55.3	51.6	35.3	29.0

533
 534 ¹ Toronto3 includes data from all three Toronto measurement sites. Toronto2 includes only data from the Gage Institute and Judson &
 535 Etona because O₃ data were not available from Junction Triangle.

536 ² Ozone data have been aggregated to 24-hour concentrations contemporaneous with PAH measurements.

537
 538 The COVs for ozone and total suspended particles (TSP) have also been included in
 539 Table 2 as comparative gaseous and particulate pollutants, respectively. Both vary less
 540 between sites in the same grid square than do PAHs. Ozone and a portion of TSP are
 541 secondary pollutants created by the mixing and reaction of precursor compounds. The
 542 atmospheric residence times required for their creation is consistent with a smoothing of
 543 the spatial variability in their concentrations though ozone variability is further
 544 complicated by reactions with NO_x near emissions from mobile sources. Conversely,
 545 unsubstituted PAHs are primary pollutants whose concentrations would be expected to
 546 vary in space over a finer resolution when multiple sources are found close by.

547
 548 The results presented above suggest that a 42-km spatial resolution is not sufficiently fine
 549 to represent PAH concentrations in areas close to sources such as cities and industrial
 550 areas if an average model accuracy better than an order of magnitude is desired.
 551 AURAMS modelling of fine particulate matter has shown substantial improvement when
 552 grid spacing has been reduced to 2.5 km (Stroud et al., 2011), and similar results can be
 553 expected for the modelling of PAHs. No 42-km model grid squares in rural or
 554 background areas away from sources contain multiple measurement stations and, as a
 555 result, a comparison cannot be made for these areas. However, it is expected that spatial

556 variation in PAH concentrations will be less in such areas and, as such, a 42-km
557 resolution model may be sufficient there.

558

559 **3.2 Particle/Gas Partitioning**

560

561 As noted in Section 3.1, the choice of partitioning expression (JP or DE) had little effect
562 on the simulation of total PAH concentrations. This implies that the partitioning from
563 each approach is sufficiently similar that regional-scale differences in removal rates
564 between gaseous and particulate PAHs have little effect. However, differences between
565 the two expressions with respect to simulating phase-resolved concentrations were noted.

566

567 **3.2.1 Overall Spatiotemporal Domain**

568

569 Figure 5 shows frequency distributions of the ratios of individual modelled-to-measured
570 particulate fraction for all data pairs available to the model evaluation. Note that only the
571 eight IADN stations are included since the gas and particle phases are analysed separately
572 only at those sites.

573

574 Figure 5 shows that PAH particulate fraction is underestimated for all species except
575 BaP. The degree of underestimation decreases with increasing molecular weight. The
576 particulate fractions of volatile PHEN and ANTH (178 g mol^{-1}) are underestimated by
577 approximately two orders of magnitude whereas equipartitioning BaA and C+T (228 g
578 mol^{-1}) have particulate fractions that are underestimated by only a factor of two. A
579 similar pattern appears when examining the partition coefficient, K_p (not shown).

580

581 For all species other than BaP, Dachs-Eisenreich partitioning performs slightly better
582 than Junge-Pankow partitioning in simulating measured particulate fractions. The all-site
583 median particulate fraction simulated using DE is between 1.1 (PYR) and 2.9 (ANTH)
584 times higher than that using JP. However, the performance of the partitioning
585 expressions is highly dependent on the physico-chemical property values used. For
586 example, estimated soot-air partition coefficients vary by more than an order of
587 magnitude (Galarneau et al., 2006) and translate directly to variations in predicted
588 partitioning by the Dachs-Eisenreich expression. For Junge-Pankow partitioning, the
589 value of the constant, c , in Eq. 1 and the estimation of aerosol surface area also introduce
590 uncertainties. A full analysis of the sensitivity of modelled partitioning is beyond the
591 scope of this paper and is explored in a separate publication (Galarneau et al., in prep.).

592

593 **3.2.2 Site-Specific Performance**

594

595 As was the case for total concentration, there is substantial variability in the simulation of
596 partitioning between sites. Figure 6 shows the variation in frequency distribution of
597 individual modelled-to-measured particulate fraction for fluoranthene using Dachs-
598 Eisenreich partitioning. Model performance for particulate fraction simulation is better at
599 urban (Chicago) or urban-influenced (Sturgeon Point, Egbert) sites than at those that are
600 remote (Eagle Harbor). An analysis of measured partitioning at IADN stations
601 (Galarneau et al., 2006) found that the proportionality between partitioning and volatility
602 varied between sites, and in some cases, over the annual cycle. Volatility is included in

603 both the JP (through p_L^0) and DE (through K_{OA} and K_{SA}) partitioning expressions and the
604 proportionality between it and partitioning magnitude is much smaller in model outputs
605 than in measurements. As noted earlier, factors involved in the performance of model
606 partitioning such as modelled particulate matter concentration and composition are
607 explored in a separate publication (Galarnau et al., in prep.)

608

609 **4. Conclusions**

610

611 This study described the first known modelling results for atmospheric PAHs at the
612 regional scale over North America. Predictions from the AURAMS-PAH model were
613 compared to roughly 5,000 24-hour average PAH measurements from 45 sites, eight of
614 which also provided data on particle/gas partitioning which had been modelled using two
615 different partitioning schemes.

616

617 The evaluation of the model is key to determining its potential utility as an input for
618 estimating the impacts of PAH inhalation exposure on human health. Annual average
619 modelled total (gas + particle) concentrations were statistically indistinguishable from
620 measured values for fluoranthene, pyrene and benz[a]anthracene, indicating the model's
621 potential utility for providing inputs to health impact estimation for these species. The
622 model annual average concentrations for phenanthrene, anthracene and
623 chrysene+triphenylene were biased low. For these species, the negative bias would have
624 to be considered if used as inputs to human health impact estimates as the model in its
625 present form underestimates long-term exposure.

626

627 The utility of the model for prediction purposes may also be considered on a day-to-day
628 basis though this is less relevant to the chronic health effects associated with carcinogenic
629 PAHs. The model simulated total PAH concentrations to the correct order of magnitude
630 64-86% of the time. That level of accuracy must be considered when assessing human
631 health impacts; annual exposure estimates are likely of more utility with the model in its
632 current state.

633

634 The partitioning approach chosen did not have a significant impact on the model results
635 for total concentrations though differences resulting from the choice of parametrization
636 approached the 95% significance level for benzo[a]pyrene. At this time, neither of the
637 two approaches used here provided a clear advantage for simulation accuracy of total
638 concentrations.

639

640 As a first work of this nature, the analysis has suggested several avenues for further
641 model development and improvement. Improved temporal emissions estimates for PAHs
642 are key to improving model simulations of these species; simulated PAHs showed less
643 temporal variability than the measurements. The reactions of particulate PAH species
644 with atmospheric oxidants should given further consideration since the more reactive
645 species were overestimated in the current model. Model resolution has been shown to be
646 a key factor in improving air pollution estimates in areas with high human exposures.
647 While the 42-km horizontal grid spacing used in this study is finer than that used in
648 global models, it was insufficient to capture the distribution of concentrations in densely
649 populated areas. A more detailed analysis of the factors influencing modelled

650 particle/gas partitioning is needed to improve the distribution of PAHs between the gas
651 and particle phases in the atmosphere given that both partitioning schemes used here
652 showed increasing negative biases for particle-bound PAH concentrations of increasing
653 volatility.

654

655 **Acknowledgements**

656

657 The authors would like to acknowledge the contributions of the AURAMS team at
658 Environment Canada, in particular Balbir Pabla, Craig Stroud, Wanmin Gong, and
659 Sunling Gong, as well as Sylvie Gravel. They thank Philip Cheung and Keith Wong for
660 their efforts in generating the maps of model output PAH concentrations. They also
661 thank Nathalie Mayrand (Rio Tinto Alcan) for sharing measurement data from the
662 Kitimat area. Finally, the authors thank Terry Bidleman and Miriam Diamond for their
663 guidance and support at the outset of this project.

664

665
666
667
668
669
670
671
672
673
674
675
676
677
678
679
680
681
682
683
684
685
686
687
688
689
690
691
692
693
694
695
696
697
698
699
700
701
702
703
704
705
706
707
708
709
710
711

References

- Aulinger, A., Matthias, V., and Quante, M.: Introducing a partitioning mechanism for PAHs into the Community Multiscale Air Quality modeling system and its application to simulating the transport of benzo[a]pyrene over Europe, *J. Appl. Met. Clim.*, 46, 1718-1730, 2007.
- Bamford, H.A., Poster, D.L., and Baker, J.E.: Temperature dependence of Henry's Law constants of thirteen polycyclic aromatic hydrocarbons between 4°C and 31°C, *Environ. Toxicol. Chem.*, 18, 1905-1912, 1999.
- Behymer, T.D. and Hites, R.A.: Photolysis of polycyclic aromatic hydrocarbons adsorbed on simulated atmospheric particulates, *Environ. Sci. Technol.*, 19, 1004-1006, 1985.
- Bidleman, T.F.: Atmospheric processes: Wet and dry deposition of organic compounds are controlled by their vapor-particle partitioning, *Environ. Sci. Technol.*, 22, 361-367, 1988.
- Bieser, J., Aulinger, A., Matthias, V., and Quante, M.: Impact of emission reductions between 1980 and 2020 on atmospheric benzo[a]pyrene concentrations over Europe. *Water Air Soil Pollut.*, 223, 1393-1414, 2012.
- Blanchard, P., Audette, C.V., Hulting, M.L., Basu, I., Brice, K.A., Backus, S.M., Dryfhout-Clark, H., Froude, F., Hites, R.A., Neilson, M., and Wu, R.: Atmospheric deposition of toxic substances to the Great Lakes: IADN results through 2005, ISBN En56-146/2005E, Environment Canada and US EPA, Toronto, 2008.
- Côté, J., Desmarais, J.-G., Gravel, S., Méthot, A., Patoine, A., Roch, M., and Staniforth, A.: The operational CMC-MRB Global Environment Multiscale (GEM) model: Part I. Design considerations and formulation, *Mon. Weather Rev.*, 126, 1373-1395, 1998.
- Côté, J., Desmarais, J.-G., Gravel, S., Méthot, A., Patoine, A., Roch, M., and Staniforth, A.: The operational CMC-MRB Global Environment Multiscale (GEM) model: Part II. Results, *Mon. Weather Rev.*, 126, 1397-1418, 1998.
- Dachs, J. and Eisenreich, S.J.: Adsorption onto aerosol soot carbon dominates gas-particle partitioning of polycyclic aromatic hydrocarbons, *Environ. Sci. Technol.*, 34, 3690-3697, 2000.
- Diamond, M.L., Gingrich, S.E., Fertuck, K., McCarry, B.E., Stern, G.A., Billeck, B., Grift, B., Brooker, D., and Yager, T.D.: Evidence for organic film on an impervious urban surface: characterization and potential teratogenic effects, *Environ. Sci. Technol.*, 34, 2900-2908, 2000.
- District of Kitimat: Kitimat, British Columbia Community Profile, District of Kitimat, B.C. 2009. <http://www.kitimat.ca/assets/Residents/PDFs/community-profile.pdf>

712 Environment Canada and Health Canada: Canadian Environmental Protection Act:
713 Priority Substances List Assessment Report: Polycyclic Aromatic Hydrocarbons,
714 Government of Canada, Ottawa, ON, Cat. No. En40-215/42E, 66 pp., 1994.
715
716 Environment Canada: Historical emission trends for benzo[a]pyrene in Canada
717 (kilograms), [http://www.ec.gc.ca/pdb/websol/emissions/ap/ap_result_e.cfm?year=1985-](http://www.ec.gc.ca/pdb/websol/emissions/ap/ap_result_e.cfm?year=1985-2007&substance=bap&location=CA§or=&submit=Search)
718 [2007&substance=bap&location=CA§or=&submit=Search](http://www.ec.gc.ca/pdb/websol/emissions/ap/ap_result_e.cfm?year=1985-2007&substance=bap&location=CA§or=&submit=Search), last access: 28 September
719 2012.
720
721 Esteve, W., Budzinski, H. and Villenave, E.: Relative rate constants for the
722 heterogeneous reactions of NO₂ and OH radicals with polycyclic aromatic hydrocarbons
723 adsorbed on carbonaceous particles. Part 2: PAHs adsorbed on diesel particulate exhaust
724 SRM 1650a, Atmos. Environ., 40, 201-211, 2006.
725
726 Finizio, A., Mackay, D., Bidleman, T. and Harner, T.: Octanol-air partition coefficient as
727 a predictor of partitioning of semi-volatile organic chemicals to aerosols, Atmos.
728 Environ., 31, 2289-2296, 1997.
729
730 Friedman, C.L. and Selin, N.E.: Long-range atmospheric transport of polycyclic aromatic
731 hydrocarbons: a global 3-D model analysis including evaluation of arctic sources,
732 Environ. Sci. Technol, 46, 9501-9510, 2012.
733
734 Galarneau, E. Source specificity and atmospheric processing of airborne PAHs:
735 implications for source apportionment, Atmos. Environ, 42, 8139-8149, 2008.
736
737 Galarneau, E., Bidleman, T.F., and Blanchard, P.: Seasonality and interspecies
738 differences in particle/gas partitioning of PAHs observed by the Integrated Atmospheric
739 Deposition Network (IADN), Atmos. Environ, 40, 182-197, 2006.
740
741 Galarneau, E. and Dann, T.: Air toxics in Canada (ATiC): preliminary scoping report,
742 Environment Canada, Toronto, ON, 24 pp., 2011.
743
744 Galarneau, E. et al.: Evaluation of particle/gas partitioning in a regional air quality model
745 (AURAMS-PAH), in preparation.
746
747 Galarneau, E., Makar, P.A., Sassi, M., and Diamond, M.L.: Estimation of atmospheric
748 emissions of six semivolatile polycyclic aromatic hydrocarbons in southern Canada and
749 the United States by use of an emissions processing system, Environ. Sci. Technol, 41,
750 4205-4213, 2007.
751
752 Gong, S. L., Barrie, L.A., Blanchet, J.-P., von Salzen, K., Lohmann, U., Lesins, G.,
753 Spacek, L., Zhang, L.M., Girard, E., Lin, H., Leaitch, R., Leighton, H., Chylek, P., and
754 Huang, P.: Canadian Aerosol Module: A size-segregated simulation of atmospheric
755 aerosol processes for climate and air quality models. 1. Module development, J. Geophys.
756 Res., 108, 4007, doi:10.1029/2001JD002002, 2003a.
757

758 Gong, S. L., Barrie, L. A., and Lazare, M.: Canadian Aerosol Module (CAM): A size-
759 segregated simulation of atmospheric aerosol processes for climate and air quality models
760 2. Global sea-salt aerosol and its budgets, *J. Geophys. Res.*, 107, 4779,
761 doi:10.1029/2001JD002004, 2003b.

762

763 Gong, W., Dastoor, A.P., Bouchet, V.S., Gong, S., Makar, P.A., Moran, M.D., Pabla, B.,
764 Ménard, S., Crevier, L.-P., Cousineau, S., and Venkatesh, S.: Cloud processing of gases
765 and aerosols in a regional air quality model (AURAMS), *Atmos. Res.*, 82, 248-275, 2006.
766

767 Gusev, A.; Dutchak, S., Rozovskaya, O., Shatalov, V., Sokovykh, V., Vulykh, N., Aas,
768 W., Breivik, K.: Persistent organic pollutants in the environment, EMEP Status Report
769 3/2011, NILU and MSC-East, 2011.

770

771 Hafner, W.D., Carlson, D.L., and Hites, R.A.: Influence of local human population on
772 atmospheric polycyclic aromatic hydrocarbon concentrations, *Environ. Sci. Technol.*, 39,
773 7374-7379, 2005.

774

775 Halsall, C.J., Sweetman, A.J., Barrie, L.A., and Jones, K.C.: Modelling the behaviour of
776 PAHs during atmospheric transport from the UK to the Arctic, *Atmos. Environ.*, 35, 255-
777 267, 2001.

778

779 Hoff, R.M., Strachan, W.M.J., Sweet, C.W., Chan, C.H., Shackleton, M., Bidleman, T.F.,
780 Brice, K.A., Burniston, D.A., Cussion, S., Gatz, D.F., Harlin, K., and Schroeder, W.H.:
781 Atmospheric deposition of toxic chemicals to the Great Lakes: a review of data through
782 1994, *Atmos. Environ.*, 30, 3505-3527, 1996.

783

784 Hung, H., Blanchard, P., Halsall, C.J., Bidleman, T.F., Stern, G.A., Felin, P., Muir,
785 D.C.G., Barrie, L.A., Jantunen, L.M., Helm, P.A., Ma, J., and Konoplev, A.: Temporal
786 and spatial variabilities in atmospheric polychlorinated biphenyls (PCBs), organochlorine
787 (OC) pesticides and polycyclic aromatic hydrocarbons (PAHs) in the Canadian Arctic:
788 results from a decade of monitoring, *Sci. Tot. Environ.*, 342, 119-144, 2005.

789

790 Inomata, Y., Kajino, M., Sato, K., Ohara, T., Kurokawa, J.-I., Ueda, H., Tang, N.,
791 Hayakawa, K., Ohizumi, T., and Akimoto, H.: Emission and atmospheric transport of
792 particulate PAHs in Northeast Asia, *Environ. Sci. Technol.*, 46, 4941-4949, 2012.

793

794 International Agency for Research on Cancer: IARC Monographs on the Evaluation of
795 Carcinogenic Risks to Humans: VOLUME 92: Some Non-heterocyclic Polycyclic
796 Aromatic Hydrocarbons and Some Related Exposures, IARC, Lyon, France, 2010.

797

798 Jonker, M.T.O. and Koelmans, A.A.: Sorption of polycyclic aromatic hydrocarbons and
799 polychlorinated biphenyls to soot and soot-like materials in the aqueous environment:
800 mechanistic considerations, *Environ. Sci. Technol.*, 36, 3725-3734, 2002.

801

802 Jones, K.C.: Observations on long-term air-soil exchange of organic contaminants,
803 *Environ. Sci. & Pollut. Res.*, 1, 172-177, 1994.

804

805 Junge, C.E.: Basic considerations about trace constituents in the atmosphere as related to
806 the fate of global pollutants, in: *Fate of Pollutants in the Air and Water Environments*,
807 Suffet, I.H. (Ed.) Wiley, New York, 7-25, 1977.

808

809 Kelly, F.J. and Fussell, J.: Review: Size, source and chemical composition as
810 determinants of toxicity attributable to ambient particulate matter, *Atmos. Environ.*, 60,
811 504-526, 2012.

812

813 Kelly, J., Makar, P.A., and Plummer, D.A.: Projections of mid-century summer air-
814 quality for North America: effects of changes in climate and precursor emissions,
815 *Atmos. Chem. Phys.*, 12, 5367-5390, 2012.

816 Kwamena, N.-O.A., Thornton, J.A., and Abbatt, J.P.D.: Kinetics of surface-bound
817 benzo[a]pyrene and ozone on solid organic and salt aerosols, *J. Phys. Chem. A*, 108,
818 11626-11634, 2004.

819

820 Lammel, G., Sehili, A.M., Bond, T.C., Feichter, J., and Grassl, H.: Gas/particle
821 partitioning and global distribution of polycyclic aromatic hydrocarbons: a modelling
822 approach, *Chemosphere*, 76, 98-106, 2009.

823

824 Lang, C., Tao, S., Liu, W., Zhang, Y., and Simonich, S.: Atmospheric transport and
825 outflow of polycyclic aromatic hydrocarbons from China, *Environ. Sci. Technol.*, 42,
826 5196-5201, 2008.

827

828 Lang, C., Tao, S., Zhang, G., Fu, J., and Simonich, S.: Outflow of polycyclic aromatic
829 hydrocarbons from Guangdong, southern China, *Environ. Sci. Technol.*, 41, 8370-8375,
830 2007.

831

832 Liu, S., Tao, S., Liu, W., Liu, Y., Dou, H., Zhao, J., Wang, L., Wang, J., Tian, Z., and
833 Gao, Y.: Atmospheric polycyclic aromatic hydrocarbons in north China: a winter-time
834 study, *Environ. Sci. Technol.*, 41, 8256-8261, 2007.

835

836 Mackay, D., Shiu, W.Y., Ma, K.-C., and Lee, S.C.: *Handbook of physical-chemical
837 properties and environmental fate for organic chemicals. Vol. 1: Introduction and
838 hydrocarbons.* Taylor and Francis, Boca Raton, FL, USA, 2006.

839

840 Makar, P.A., Zhang, J., Gong, W., Stroud, C., Sills, D., Hayden, K.L., Brook, J., Levy, I.,
841 Mihele, C., Moran, M.D., Tarasick, D.W., and He, H.: Mass tracking for chemical
842 analysis: the causes of ozone formation in southern Ontario during BAQS-Met 2007,
843 *Atmos. Chem. Phys.*, 10, 11151-11173, 2010.

844

845 Matthias, V., Aulinger, A., and Quante, M.: CMAQ simulations of the benzo[a]pyrene
846 distribution over Europe for 200 and 2001, *Atmos. Environ.*, 43, 4078-4086, 2009.

847

848 McDow, S.R.: Sampling artefact errors in gas/particle partitioning measurements, in: Gas
849 and Particle Phase Measurements of Atmospheric Organic Compounds, Lane, D.A. (Ed.),
850 Gordon and Breach Science Publishers, Canada, 105-126, 1999.

851

852 McKeen, S., Chung, S.H., Wilczak, J., Grell, G., Djalalova, I., Peckham, S., Gong, W.,
853 Bouchet, V., Moffet, R., Tang, Y., Carmichael, G.R., Mathur, R., and Yu, S.: Evaluation
854 of several real-time PM_{2.5} forecast models using data collected during the
855 ICARTT/NEAQS 2004 field study, *J. Geophys. Res.*, 112, D10S20,
856 doi:10.1029/2006JD007608, 2007.

857

858 Menichini, E.: On-filter degradation of particle-bound benzo[a]pyrene by ozone during
859 air sampling: a review of the experimental evidence of an artefact, *Chemosphere*, 77,
860 1275-1284, 2009.

861

862 Odabasi, M., Cetin, E., and Sofuoglu, A.: Determination of octano-air partition
863 coefficients and supercooled liquid vapour pressures of PAHs as a function of
864 temperature: application to gas-particle partitioning in an urban atmosphere, *Atmos.*
865 *Environ.*, 40:6615-6625, 2006.

866

867 Offenberg, J.H. and Baker, J.E.: Aerosol size distributions of polycyclic aromatic
868 hydrocarbons in urban and over-water atmospheres, *Environ. Sci. Technol.*, 33, 3324-
869 3331, 1999.

870

871 Pankow, J.F.: Review and comparative analysis of the theories on partitioning between
872 the gas and aerosol particulate phases in the atmosphere, *Atmos. Environ.*, 21, 2275-
873 2283, 1987.

874

875 Pöschl, U., Letzel, T., Schauer, C., and Niessner, R.: Interaction of ozone and water
876 vapor with spark discharge soot aerosol particles coated with benzo[a]pyrene: O₃ and
877 H₂O adsorption, benzo[a]pyrene degradation, and atmospheric implications, *J. Phys.*
878 *Chem. A*, 105, 4029-4041, 2001.

879

880 Prevedouros, K., Jones, K.C., and Sweetman, A.J.: Modelling the atmospheric fate and
881 seasonality of polycyclic aromatic hydrocarbons in the UK, *Chemosphere*, 56, 195-208,
882 2004.

883

884 Prevedouros, K., Palm-Cousins, A., Gustafsson, Ö., and Cousins, I.T.: Development of a
885 black carbon-inclusive multi-media model: application for PAHs in Stockholm,
886 *Chemosphere*, 70, 607-615, 2008.

887

888 Reid, R.C., Prausnitz, J.M., and Poling, B.E.: The properties of gases and liquids.
889 McGraw-Hill, Toronto, 1987.

890

891 Sehili, A.M. and Lammel, G.: Global fate and distribution of polycyclic aromatic
892 hydrocarbons emitted from Europe and Russia, *Atmos. Environ.*, 41, 8301-8315, 2007.

893

894 Shatalov, V., Gusev, A., Dutchak, S., Holoubek, I., Mantseva, E., Tozovskaya, O.,
895 Sweetman, A., Strukov, B., and Vulykh, N.: Modelling of POP contamination in
896 European region: evaluation of the model performance, EMEP/MSC-E Technical Report
897 7/2005, 2005.

898

899 Shiraiwa, M., Garland, R.M., and Pöschl, U.: Kinetic double layer model of aerosol
900 surface chemistry and gas-particle interactions (K2-SURF): degradation of polycyclic
901 aromatic hydrocarbons exposed to O₃, NO₂, H₂O, OH and NO₃, Atmospheric
902 Chemistry and Physics, 9, 9571-9586, 2009.

903

904 Smyth, S.C., Jiang, W., Roth, H., Moran, M.D., Makar, P.A., Yang, F., Bouchet, V.S.,
905 and Landry, H.: A comparative performance evaluation of the AURAMS and CMAQ air-
906 quality modelling systems, Atmos. Environ., 43, 1059-1070, 2009.

907

908 Solazzo, E., Bianconi, R., Vautard, R., Appel, K.W., Moran, M.D., Hogrefe, C.,
909 Bessagnet, B., Brandt, J., Christensen, J.H., Chemel, C., Coll, I., Denier van der Gon, H.,
910 Ferreira, J., Forkel, R., Francis, X.V., Grell, G., Grossi, P., Hansen, A.B., Jeričević, A.,
911 Kraljević, L., Miranda, A.I., Nopmongcol, U., Pirovano, G., Prank, M., Riccio, A.,
912 Sartelet, K.N., Schaap, M., Silver, J.D., Sokhi, R.S., Vira, J., Werhahn, J., Wolke, R.,
913 Yarwood, G., Zhang, J., Rao, S.T., and Galmarini, S.: Model evaluation and ensemble
914 modelling of surface-level ozone in Europe and North America in the context of
915 AQMEII. Atmos. Environ., 53, 60-74, 2012.

916

917 Statistics Canada: Population of census metropolitan areas,
918 <http://www40.statcan.ca/l01/cst01/demo05a-eng.htm>, last access: 25 August 2011.

919

920 Stroud, C., Makar, P.A., Moran, M.D., Gong, W., Gong, S., Zhang, J., Hayden, K.,
921 Mihele, C., Brook, J.R., Abbatt, J.P.D., and Slowik, J.G.: Impact of model grid spacing
922 on regional- and urban- scale air quality predictions of organic aerosol, Atmos. Chem.
923 Phys., 11, 3107-3118, 2011.

924

925 U.S. E.P.A.: Estimation program interface (EPI) suite.,
926 <http://www.epa.gov/opptintr/exposure/pubs/episuite.htm>, last access: 2 June 2006.

927

928 U.S. E.P.A.: The Clean Air Act Amendments of 1990 List of Hazardous Air Pollutants.,
929 <http://www.epa.gov/ttnatw01/orig189.html>, last access: 28 September 2012.

930

931 U.S. E.P.A.: TRI Explorer Web Tool,
932 http://iaspub.epa.gov/triexplorer/tri_release.chemical, last access: 28 September 2012.

933

934 US EPA: National-scale air toxics assessment (NATA). Summary of results for the 2005
935 national-scale assessment., http://www.epa.gov/ttn/atw/nata2005/05pdf/sum_results.pdf,
936 last access: 28 September 2012.

937

938 Van Jaarsveld, J.A., Van Pul, W.A.J., and De Leeuw, F.A.A.M.: Modelling transport and
939 deposition of persistent organic pollutants in the European region, *Atmos. Environ.*, 31,
940 1011-1024, 1997.

941

942 Yaffe, D., Cohen, Y., Arey, J., and Grosovsky, A.J.: Multimedia analysis of PAHs and
943 nitro-PAH daughter products in the Los Angeles Basin, *Risk Analysis*, 21, 275-294,
944 2001.

945

946 Zhang, L., Moran, M.D., Makar, P.A., Brook, J.R., and Gong, S.: Modelling gaseous dry
947 deposition in AURAMS: an unified regional air-quality modelling system, *Atmos.*
948 *Environ.*, 36, 537-560, 2002.

949

950 Zhang, Y., Shen, H., Tao, S., and Ma, J.: Modeling the atmospheric transport and outflow
951 of polycyclic aromatic hydrocarbons emitted from China, *Atmos. Environ.*, 45, 2820-
952 2827, 2011.

953

954 Zhang, Y., Tao, S., Ma, J., and Simonich, S.: Transpacific transport of benzo[a]pyrene
955 emitted from Asia: importance of warm conveyor belt and interannual variations, *Atmos.*
956 *Chem. Phys.*, 11, 18879-19009, 2011.

957

958 Zhang, Y., Tao, S., Shen, H., and Ma, J.: Inhalation exposure to ambient polycyclic
959 aromatic hydrocarbons and lung cancer risk of Chinese population, *PNAS*, 106, 21063-
960 21067, 2009.

961

962

963

964 **List of Figures**

965

966 **Figure 1:** Map of modelled (JP) annual average total (gas + particle) fluoranthene
967 concentrations (ng m^{-3}).

968

969 **Figure 2:** Map of measurement stations used in AURAMS-PAH evaluation.

970

971 **Figure 3:** All-site ensemble of modelled-to-measured concentration ratios for total (gas +
972 particle) PAHs using JP and DE partitioning expressions.

973

974 **Figure 4:** Site-specific modelled-to-measured concentration ratios for total (gas +
975 particle) fluoranthene for JP partitioning.

976

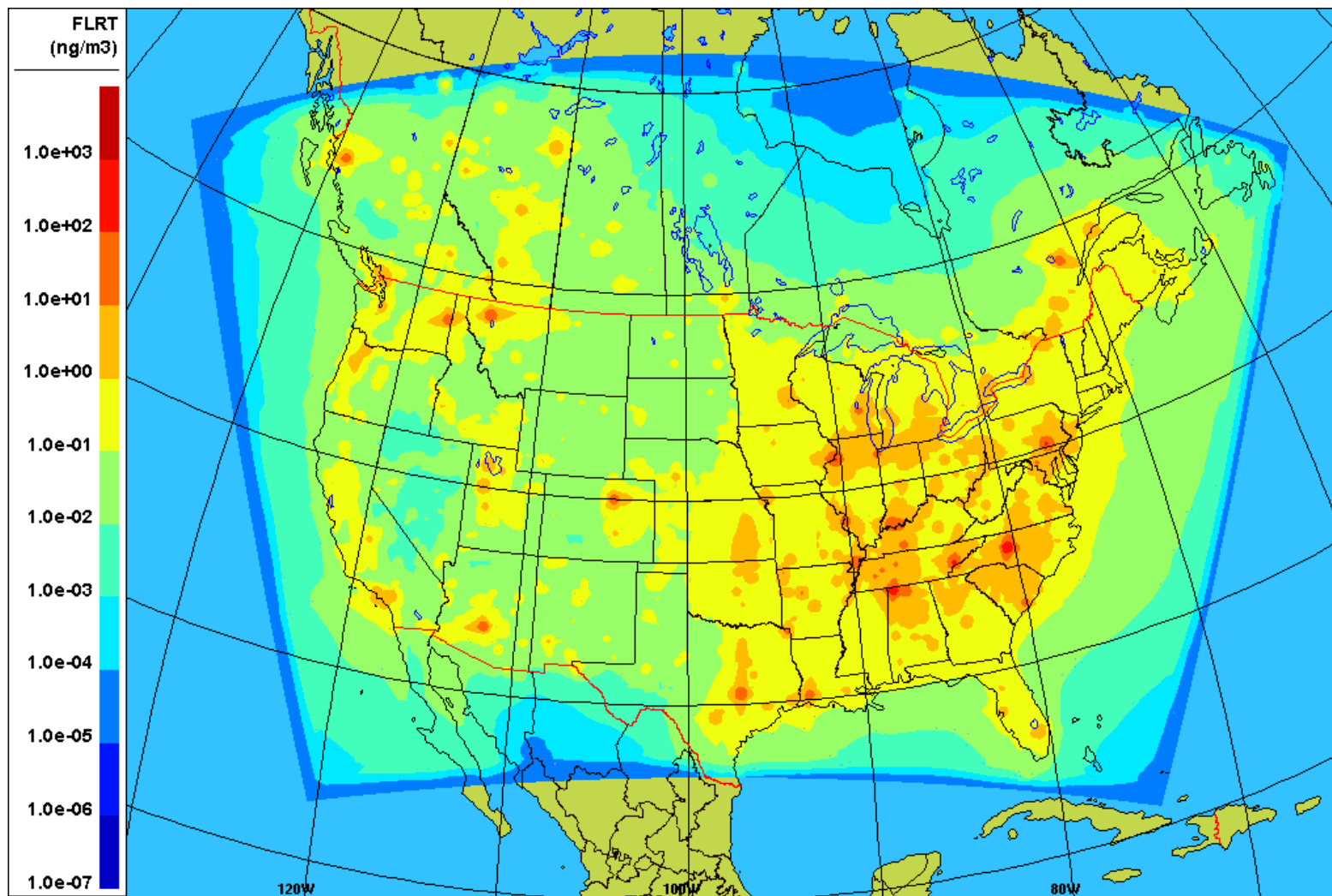
977 **Figure 5:** All-site ensemble of modelled-to-measured PAH particulate fraction ratios for
978 JP and DE partitioning expressions.

979

980 **Figure 6:** Site-specific modelled-to-measured partition coefficients for fluoranthene for
981 DE partitioning for eight IADN sites.

982

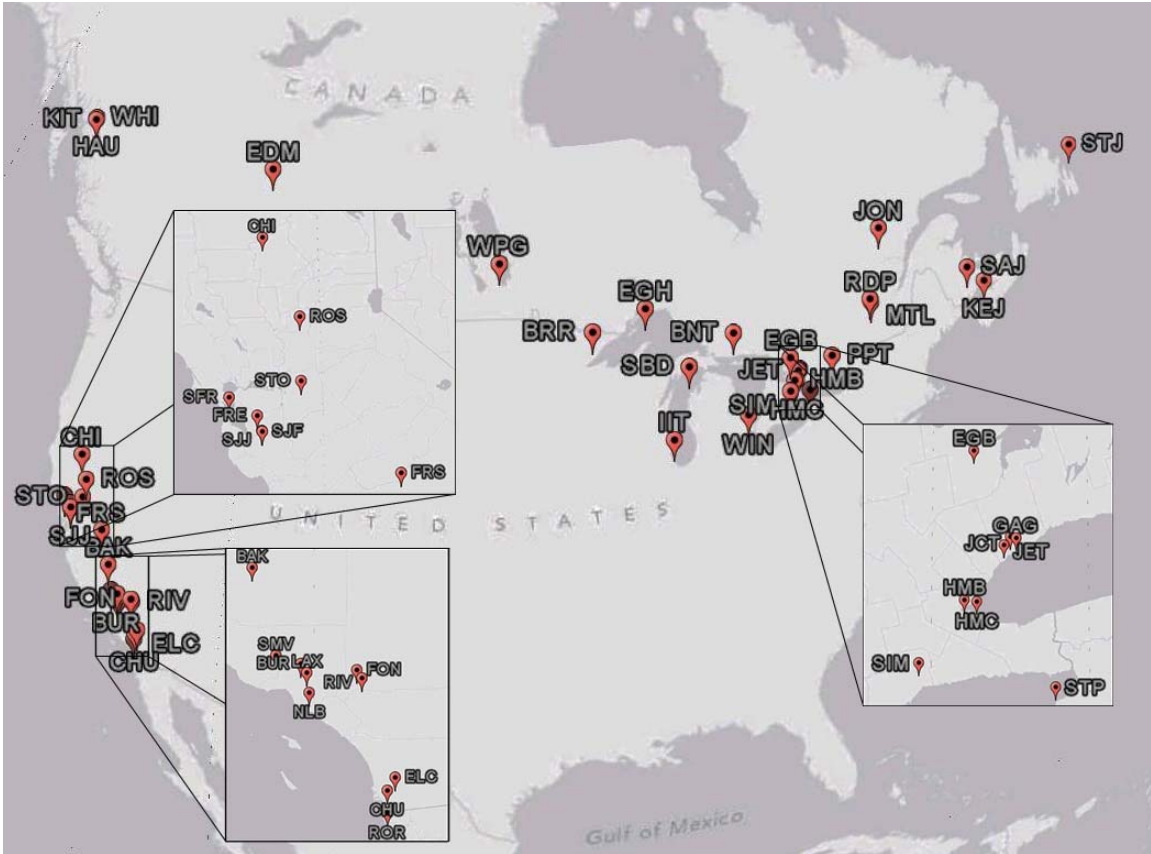
983 **Figure 1: Map of modelled (JP) annual average total (gas + particle) fluoranthene concentrations (ng m^{-3}).**
984



985

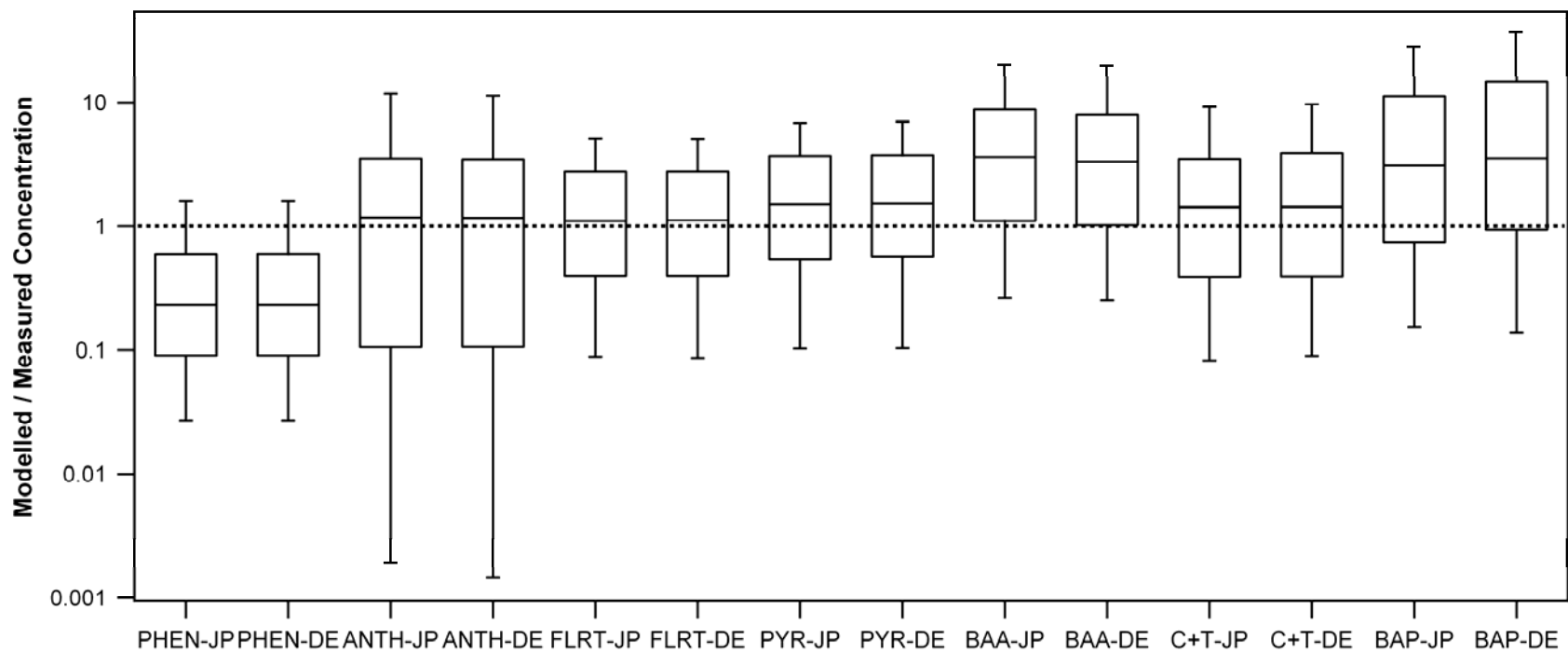
986
987

Figure 2: Map of measurement stations used in AURAMS-PAH evaluation.



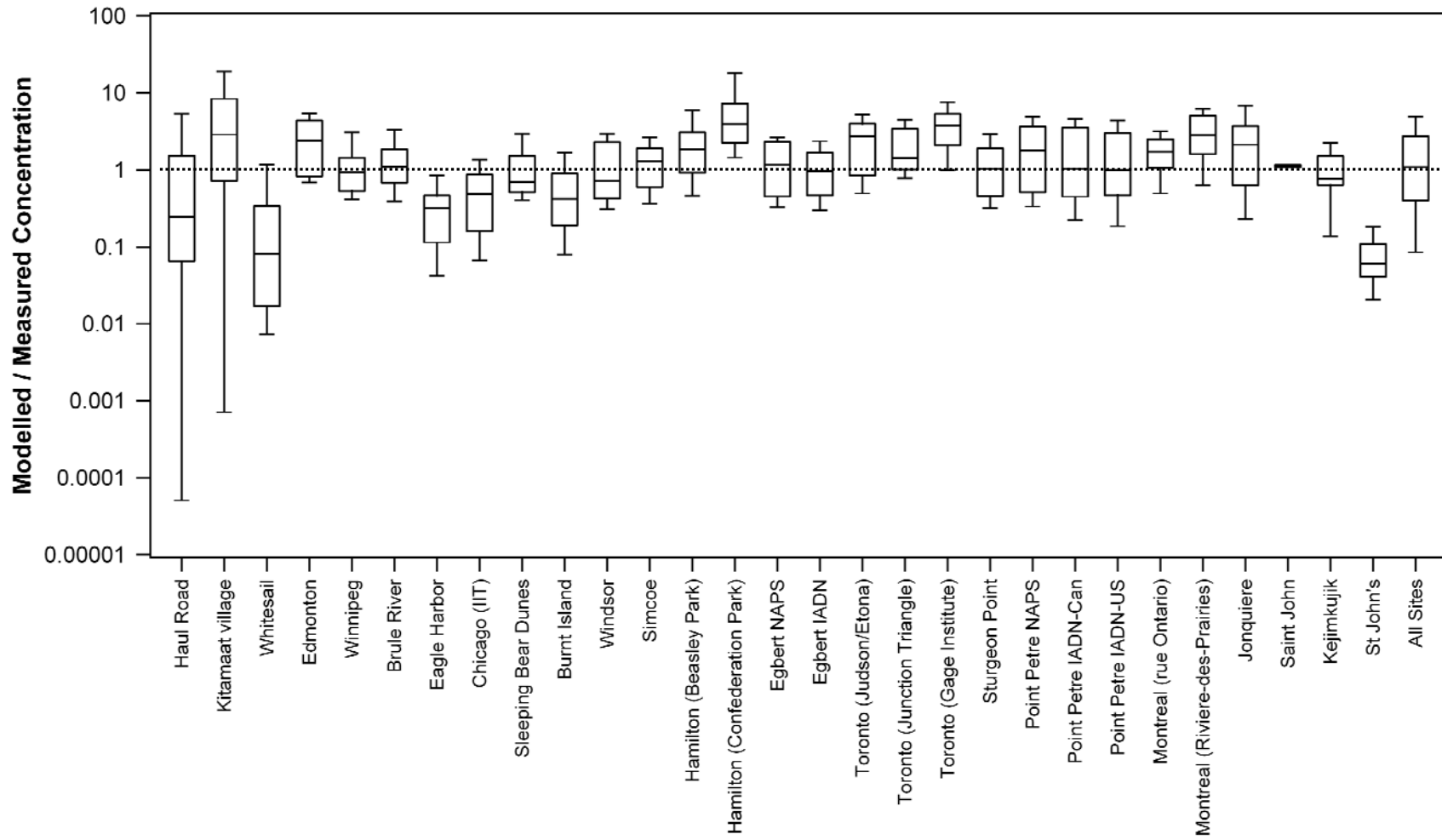
988
989

990 **Figure 3: All-site ensemble of modelled-to-measured concentration ratios for total (gas + particle) PAHs using JP and DE**
991 **partitioning expressions.**
992



993
994 N.B. Box boundaries are 25th, 50th and 75th percentile values; whiskers are 10th and 90th percentile values. JP = Junge-Pankow partitioning; DE = Dachs-
995 Eisenreich partitioning.

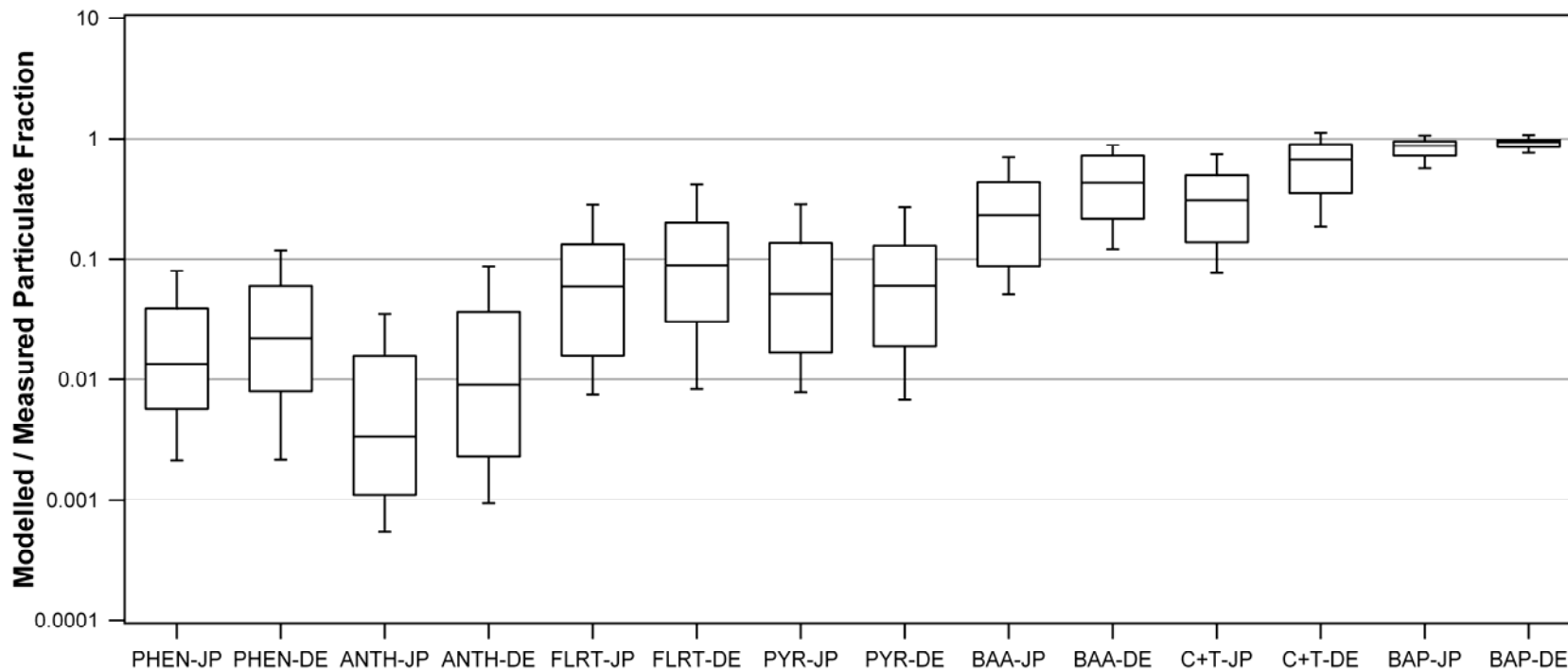
Figure 4: Site-specific modelled-to-measured concentration ratios for total (gas + particle) fluoranthene for JP partitioning



997 N.B. Box boundaries are 25th, 50th and 75th percentile values; whiskers are 10th and 90th percentile values.

998
999

Figure 5: All-site ensemble of modelled-to-measured PAH particulate fraction ratios for JP and DE partitioning expressions.

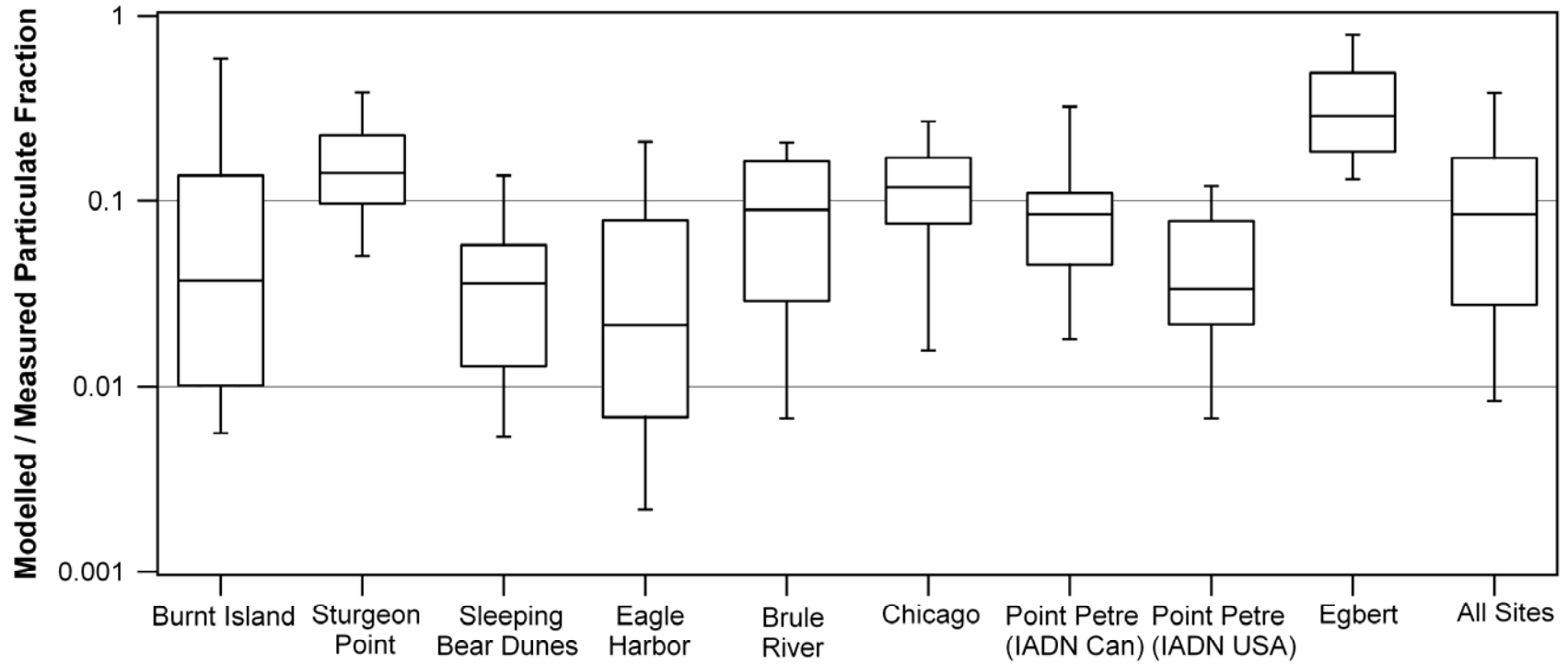


1000
1001
1002
1003
1004
1005
1006
1007

N.B. Box boundaries are 25th, 50th and 75th percentile values; whiskers are 10th and 90th percentile values. JP = Junge-Pankow partitioning; DE = Dachs-Eisenreich partitioning.

1008
1009

Figure 6: Site-specific modelled-to-measured partition coefficients for fluoranthene for DE partitioning for eight IADN sites.



1010
1011
1012
1013
1014
1015

N.B. Box boundaries are 25th, 50th and 75th percentile values; whiskers are 10th and 90th percentile values.

